Synchronization of Electro-Optically Modulated Kerr Soliton to a Chip-Scale Mode-Locked Laser PIC via Regenerative Harmonic Injection Locking

Ricardo Bustos-Ramirez, Chinmay Shirpurkar, *Graduate Student Member, IEEE*, Srinivas Pericherla, Lawrence R. Trask, Travis C. Briles, Jordan R. Stone, Su-Peng Yu, Ashish Bhardwaj, Gloria E. Hoefler, Scott B. Papp, and Peter J. Delfyett

(Top-Scored Paper)

***Abstract*—An InP-based mode-locked laser photonic integrated circuit with a repetition rate of 10 GHz is optically synchronized to a SiN microresonator-based dissipative Kerr soliton with a repetition rate of 305 GHz. The synchronization is achieved through regenerative harmonic injection locking assisted with electro-optic division which results in an optical frequency division factor of 18. The repetition rate of the dissipative Kerr soliton is stabilized through electro-optic division and transferred to the mode-locked laser, where we measure a fractional frequency instability in the repetition rate of 10^{-10} at 1 s with a $1/\tau$ trend. Furthermore, we also stabilize the repetition rate of the dissipative Kerr soliton using the mode-locked laser's repetition rate beat as a feedback point.**

***Index Terms*—Electro-optic division, kerr soliton combs, photonic integrated circuits, semiconductor mode-locked lasers.**

I. Introduction

THE field of optical frequency comb technology has grown rapidly in the past few years due to their applications spanning high-speed photonic digital signal processing [1], frequency spectroscopy [2], optical atomic clocks [3], high-speed optical interconnects [4], laser radar and ranging [5], and optical frequency synthesis [6], amongst others. The development of compact as well as chip-scale pulsed sources, such as semiconductor mode-locked lasers [7] and microresonator-based Kerr frequency combs [8] have significantly increased the potential to bring frequency comb technology out of research laboratories and into real world applications. Hence, the development of technology to realize compact, and energy-efficient frequency comb sources has become a topic of high interest in the research community.

In order to generate a fully stabilized optical frequency comb, we require absolute knowledge about two defining properties of the frequency comb, namely its carrier-envelope offset frequency and its repetition rate frequency [9]. If we can know and control both of these frequencies accurately, then we can generate a fully stabilized optical frequency comb. Acquiring knowledge of the repetition rate, which is the rate at which pulses come out of the laser, can be measured using a high-speed photodiode in front of the laser beam. On the other hand, measuring the carrier-envelope offset frequency, which arises from the difference between the phase velocity and the group velocity in the laser cavity, requires f-2f interferometry [10], which in turn requires a coherent octave of optical bandwidth.

In this work, we focus on two types of integrated pulsed sources that have the potential to generate a fully stabilized optical frequency comb, our aim is to synchronize this two types of pulsed sources with each other and stabilize their repetition rates. For the case of semiconductor mode-locked laser diodes (MLLD), their repetition rates range from 1 GHz to 10 s of GHz which can be easily detected using commercial high-speed photodiodes. Furthermore, they are electrically pumped, extremely energy efficient, and relatively simple to use. Nonetheless, the optical bandwidth coming directly out of semiconductor MLLDs ranges from 1-2 nm to 10 s of nm, and hence nonlinear optical bandwidth broadening is needed to obtain a coherent octave of optical bandwidth. Such extreme nonlinear processes become challenging for integrated semiconductor MLLDs, due to their low pulse energy, arising from GHz repetition rates and limited optical output power [11].

Manuscript received August 14, 2021; revised October 22, 2021; accepted October 27, 2021. Date of publication December 14, 2021; date of current version March 16, 2022. This work was supported in part by the DARPA DODOS HR0011-15-C-0057 National Science Fundation under Grant 1509619 R.B.R. acknowledges student support from CONACyT. *(Ricardo Bustos-Ramirez and Chinmay Shirpurkar contributed equally to this work.) (Corresponding author: Ricardo Bustos-Ramirez.)*

Ricardo Bustos-Ramirez is with CREOL, The College of Optics and Photonics, University of Central Florida, Orlando, FL 32816 USA, and also with the Infinera Corporation, Sunnyvale, CA 9408 USA (e-mail: ricardo.bustos@knights.ucf.edu).

Chinmay Shirpurkar, Srinivas Pericherla, Lawrence R. Trask, and Peter J. Delfyett are with CREOL, The College of Optics and Photonics, University of Central Florida, Orlando, FL 32816 USA (e-mail: shirpurkar.chinmay@knights.ucf.edu; srinivasvarma@knights.ucf.edu; lawrencetrask@knights.ucf.edu; delfyett@creol.ucf.edu).

Travis C. Briles, Jordan R. Stone, Su-Peng Yu, and Scott B. Papp are with the Time and Frequency Division, National Institute for Standards and Technology, Boulder, CO 80305 USA (e-mail: travis.briles@colorado.edu; jordan.stone@colorado.edu; supeng.yu@colorado.edu; scott.papp@colorado.edu).

Ashish Bhardwaj and Gloria E. Hoefler are with the Infinera Corporation, Sunnyvale, CA 9408 USA (e-mail: abhardwaj@infinera.com; ghoefler@infinera.com).

Color versions of one or more figures in this article are available at https://doi.org/10.1109/JLT.2021.3135235.

Digital Object Identifier 10.1109/JLT.2021.3135235

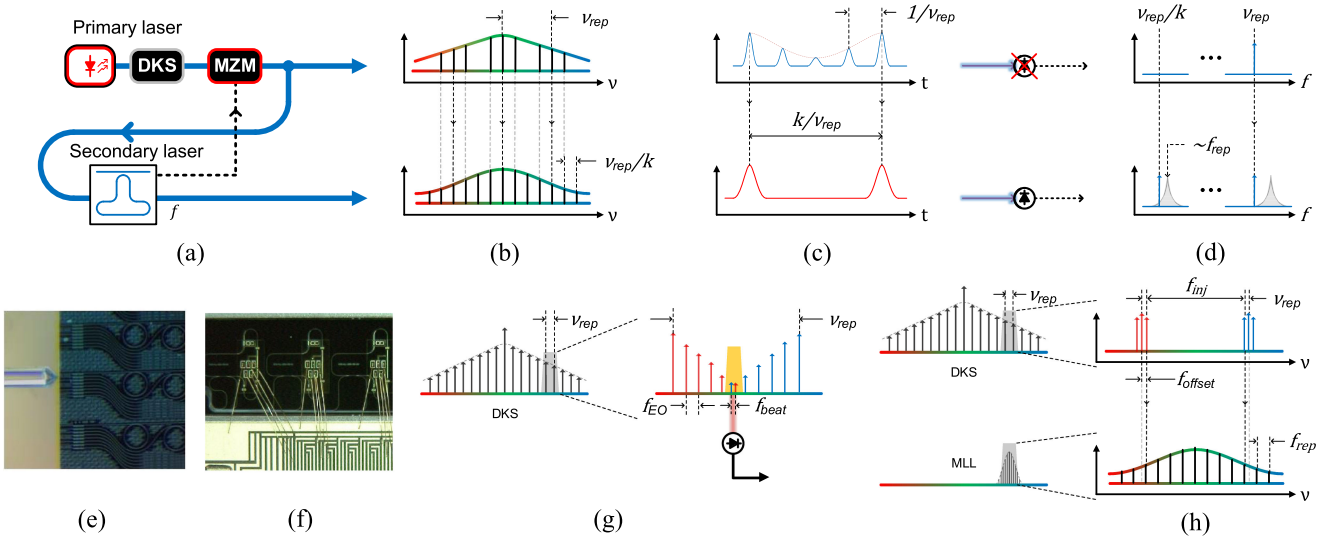

Fig. 1. (a) Fundamental concept behind RHIL, a primary OFC (DKS, comprised of a laser and a microresonator (DKS, top) with a repetition rate ν_{rep} is injected into a secondary OFC (MLL-PIC, bottom) with a repetition rate that of the subharmonic of the primary laser ($f_{rep} = \nu_{rep}/4$). Simultaneously, a COEO loop is created between the MLL and the DKS. (b) Optical spectrum of the primary (DKS) and secondary (MLL-PIC) lasers, the sidebands in the primary laser arise from the COEO loop. Pulsed behaviour (c) and RF beat of the repetition rate (d) of primary and secondary lasers. (e) SiN-based microresonator chip and tapered fiber from left. (f) Micrograph of InP-based MLL-PIC. (g) Optical axial modes of DKS with EOD showing a graphic representation of (3). (h) Optical axial modes of DKS and MLL-PIC showing a graph representation of (1) and (2).

On the other hand, thanks to precise dispersion engineering and developments in the fabrication of low-loss nonlinear waveguides, microresonator-based optical frequency combs, which can generate dissipative Kerr solitons (DKS), can be designed to produce pulses at rates of 100 s of GHz or even 1 THz. These frequency combs can span over an octave of optical bandwidth, which makes carrier-envelope offset stabilization possible [6]. Nonetheless, repetition rates of 100 s of GHz cannot be measured directly using commercial integrated photodetectors and electro-optic technology. Hence, people rely on indirect methods to measure the ultra-high repetition rates of the DKS such as electro-optic division [12], interlocked dual combs [6], and Vernier frequency division [13]. Furthermore, there are direct methods, such as the use of uni-traveling carrier photodiodes directly at 300 GHz, and frequency division using gain-switched semiconductor lasers [14].

In this work, we present a novel technique to obtain knowledge about the repetition rate frequency of a 305 GHz microresonator-based frequency comb using optical frequency division down to 10 GHz. Using regenerative harmonic injection locking (RHIL) [15] assisted by electro-optic division, we can measure the repetition rate frequency of the DKS and its repetition rate frequency instability directly at the output of an InP-based mode-locked laser photonic integrated circuit (MLL-PIC) at 10 GHz that has an integrated intracavity photodiode. We also present a modified version of our technique where we utilize the repetition rate beat signal from the MLL-PIC as a feedback point to stabilize the repetition rate frequency of the DKS at 305 GHz.

II. Fundamental Concept, Kerr Comb and MLL-PIC Introduction

The optical frequency division presented in this work is based on regenerative harmonic injection locking (RHIL) which relies on optical injection locking [16], and is an evolution of coupled opto-electronic oscillator (COEO) multi-tone injection locking technique [17], [18] that has been demonstrated for lasers at different repetition rates. In RHIL, a primary laser (microcomb), defined by $\nu_n = \nu_{CEO} + n\nu_{rep}$ is optically injected into a secondary laser (MLL-PIC), defined as $f_n = f_{CEO} + mf_{rep}$. Due to injection locking (shown in Fig. 1(a)), the injected modes from the secondary laser synchronize in frequency and phase to the injected modes of the primary laser (shown in Fig. 1(b)). Furthermore, if the secondary laser is implemented as a mode-locked laser, all the axial modes share a fixed phase relationship. This effectively links the repetition rate and carrier-envelope offset frequencies of the primary and secondary lasers, which can be described as $\nu_{rep} = kf_{rep}$ and $f_{CEO} = \nu_{CEO} + (nk - m)f_{rep}$ respectively. This results in an optical frequency division (OFD) of the primary optical frequency comb (OFC) laser by a integer factor 'k,' which can then be measured at the output of the secondary laser (shown in Fig. 1(d)). This technique has limitations for large division factors (such as $k > 10$) because the secondary laser (MLL-PIC) will have to respond to frequencies far larger than its natural repetition rate. In order to overcome this limitation, a COEO is implemented in the secondary laser. The COEO effectively serves as a pulse-picker that attenuates the pulses from the primary laser that do not match with the secondary laser, while keeping the pulses that match the secondary laser at maximum power (shown in Fig. 1(c)). Furthermore, the COEO serves to increase the cavity factor Q of the secondary laser while reducing the noise, which helps in the OFD process and improves the long-term stability of RHIL.

In this experiment, the secondary laser is implemented as an InP-based mode-locked laser photonic integrated circuit (MLL-PIC), realized as a racetrack laser in a colliding-pulse architecture. The laser consist of a passive cavity with a free spectral range (FSR) of ∼10 GHz, a gain section, a saturable

absorber (SA) that provides the means for passive mode-locking, and a high-speed intracavity absorber (IA). Furthermore, a multi-mode interference coupler (MMI) provides an input for injection locking and an output for the pulses generated in the MLL-PIC. Finally, the output port of the MMI features an external on-chip semiconductor optical amplifier (SOA) to boost the power of the output pulses. The laser is biased to operate under passive mode-locking, where the repetition rate ranges from f_{rep} ~9.98–10.03 GHz, depending on the bias conditions. A detailed description on the design and characterization of the MLL-PIC presented in this work can be found in [19]. A micro-photograph of the MLL-PIC is shown in Fig. 1(f).

The primary laser is a microresonator Kerr-based soliton optical frequency comb (a micro-photograph of the SiN microresonator used in this experiment can be found in Fig. 1(e)). In order to generate coherent dissipative Kerr solitons (DKS), the SiN-based microresonator is optically pumped with a CW laser. The Lugiato-Lefever equation which models the nonlinear dynamics in a microresonator requires the CW pump laser to be detuned to the lower-frequency side (red) of the resonance for soliton generation. As the CW pump is tuned from the blue-detuned side to the red-detuned side, there is a buildup of power in the cavity that results in noisy modulational instability combs in the cavity. As the CW pump is detuned further towards the red side, there is a sudden drop in power and the modulational instability combs collapse into coherent soliton frequency combs. The sudden drop in power as the CW pump is tuned into the soliton regime causes rapid thermal relaxation which leads to a shift in the resonance that is outside the detuning range required for soliton existence. Therefore, the frequency ramp given to the pump laser must be swept across the resonance in three parts matching the speeds of the thermal relaxation constants of the microresonator, the bus waveguide and the chip respectively [20]. The optical spectrum of the DKS generated through fast detuning of the pump frequency is shown in Fig. 2(a) in a wide span and in Fig. 2(b) in a narrow span together with the optical spectrum of the MLL-PIC under passive mode-locking.

The measured repetition rate of the DKS is ν_{rep} ~305 GHz. Hence, taking into account that we can tune the repetition rate (f_{rep}) of the MLL-PIC between f_{rep} ~9.98–10.03 GHz, there is a frequency mismatch between the MLL's repetition rate and the DKS repetition rate, for which the relation $\nu_{rep} = kf_{rep}$ is not satisfied. Therefore, the frequency spacing of the injected tones needs to be modified in order to match the optical axial modes of the MLL-PIC. This can be done through electro-optic division, that is, through adding sidebands that closely match a harmonic of the MLL-PIC's repetition rate, following

$$\nu_{rep} = f_{inj} + 2f_{offset}, \tag{1}$$

where f_{inj} represents the injected tones that match the "k^{th}" harmonic of the MLL's repetition rate (f_{rep}),

$$f_{inj} = kf_{rep}. \tag{2}$$

For example, if $\nu_{rep} = 305$ GHz and $f_{rep} = 10$ GHz, then $f_{offset} = 2.5$ GHz, and $f_{inj} = 300$ GHz with $k = 30$. This can be applied to any harmonic constant k.

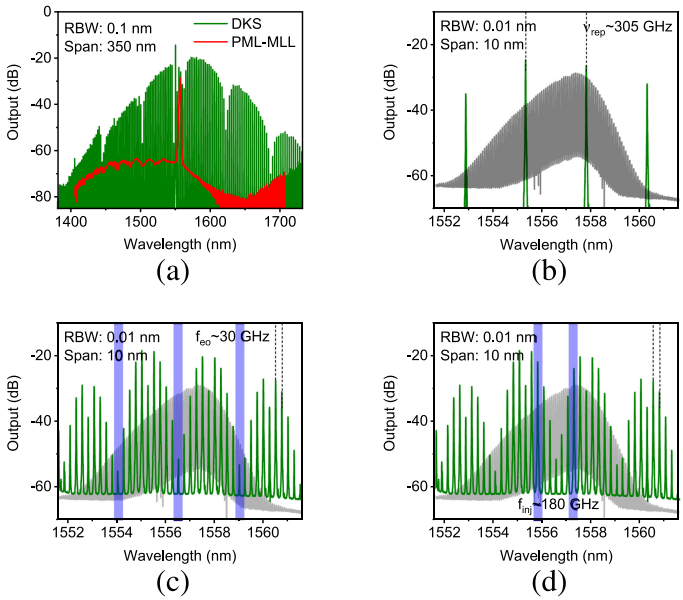

Fig. 2. Output optical spectrum of microresonator-based dispersive Kerr soliton after a notch filter to suppress the pump (olive) and MLL-PIC under PML (red) on a 350 nm span.

A graphic representation of the link between the axial modes of the DKS and MLL is shown in Fig. 1(h).

In addition, we implement electro-optic division (EOD) as an alternative technique to measure the repetition rate of the DKS (ν_{rep}). This ensures that the repetition rate of the DKS obtained through RHIL matches the repetition rate frequency obtained through a known established technique to measure the DKS' repetition rate frequency (see (1) and (2)). The EOD technique is based on passing light from the DKS through a series of electro-optic modulators driven at a frequency close to a subharmonic of the repetition rate [12], [21] of the primary DKS ($f_{EO} \sim \nu_{rep}/l$). The residual beat signal between the overlapping innermost axial modes can de used to measure the repetition rate of the DKS accurately, following

$$\nu_{rep} = lf_{EO} - f_{\text{beat}}. \tag{3}$$

A depiction of the EOD method is shown in Fig. 1(g) where $l = 10$.

III. OFD via RHIL - Experimental Setup and Result

The experimental setup used to synchronize the repetition rates of the DKS and MLL-PIC is show in in Fig. 3(a). In order to generate a stable coherent dissipative Kerr soliton (DKS), light from an ultra-narrow linewidth CW laser ($\Delta\nu$ ~10 Hz) is amplified and passed through an IQ modulator using a single-sideband suppressed-carrier configuration driven by a voltage-controlled oscillator (VCO). The voltage ramp applied to the VCO is generated by an arbitrary waveform generator (AWG) that dictates the speed and range of the frequency sweep of the laser across the resonance of the microresonator. The output of the IQ modulator is amplified to ~400 mW and passed through a tunable band-pass filter to filter amplfied spontaneous emission (ASE),, a polarization controller, a polarizer and another final

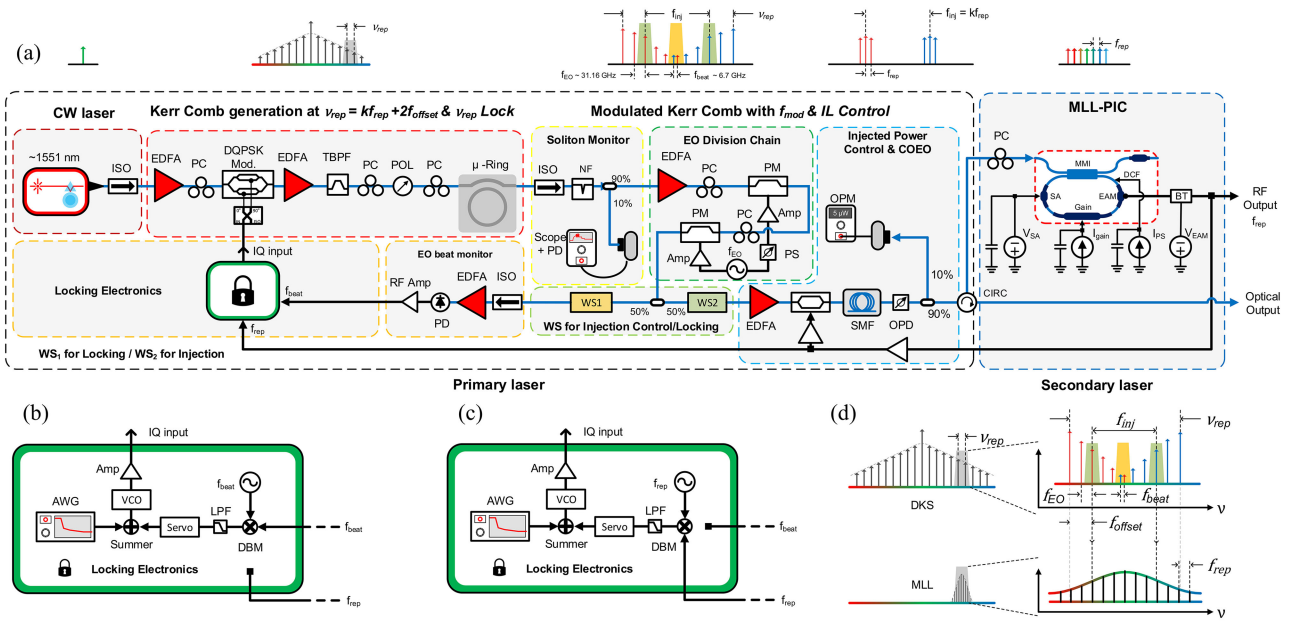

Fig. 3. (a) DKS to MLL-PIC link experimental setup at f_{inj} ~180 GHz. DQPSK: Differential quadrature phase keying modulator, TBPF: Tunable bandpass filter, NF: Notch filter, WS1: Waveshaper for EOD, WS2: Waveshaper for RHIL, OPD: Optical phase delay, AWG: Arbitraty waveform generator, VCO: Voltage controlled oscillator, LPF: Low pass filter. Summer: Differential amplifier in a summer configuration. Repetition rate locking electronics utilizing f_{beat} (b) and f_{rep} (c) as feedback signal points. (d) Pictographic representation of EOD and RHIL.

polarization controller before it is injected into a SiN microresonator with a 305 GHz free-spectral range (FSR). The output of the microresonator is passed through a notch filter that serves to suppress the optical pump and 10% of the light is sent to a power meter to monitor the optical output power of the soliton.

The soliton (DKS) output is then passed through a series of phase modulators driven at a frequency of f_{EO} ~31 GHz to perform electro-optical frequency division. The output of the electro-optically-divided DKS comb is then split equally into two paths to fulfill two purposes: 1) To have an alternative method to know and control the repetition rate of the DKS, and 2) for OFD via RHIL, as shown in Fig. 3(d).

Specifically, the first half of the power is utilized to continuously measure the repetition rate frequency of the DKS using electro-optic division (EOD) [12], [21], which serves to divide the repetition rate of the DKS ν_{rep} ~305 GHz to a repetition rate (f_{beat}) that can be measured with a commercial high-speed photodiode. The relation between the measured beat and the DKS repetition rate is:

$$\nu_{rep} = l f_{EO} - f_{\text{beat}}. \tag{4}$$

Where $l = 10$ since there are 10 axial modes (5 to each side) for each DKS optical axial mode generated through electro-optic modulation. Specifically, the modulators are driven at $f_{EO} =$ 31.16323 GHz and the overlapping innermost generated optical axial modes are isolated using a liquid crystal-on-silicon (LCoS)-based waveshaper. The isolated axial modes are then amplified and detected using a high-speed photodiode, the optical spectrum resulting from EOD can be seen in Fig. 2(c) where the isolated tones are highlighted. The resulting beat oscillating at f_{beat} ~6.7 GHz is shown in Fig. 4(a).

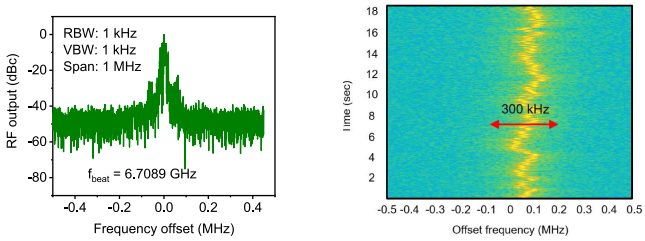

Fig. 4. (a) Electro-optic division (EOD) beat signal of DKS at f_{beat} ~6.7 GHz. (b) Spectrogram of nominal drift of DKS-EOD repetition rate beat.

Furthermore, Fig. 4(b) shows a spectrogram of the beat signal at f_{beat} where a drift of less than 300 kHz around its center is observed, whereas the f_{beat} oscillates at a frequency of ~6.7089 GHz. This yields a repetition rate of the DKS oscillating at a frequency of $\nu_{rep} = 10 f_{EO} - f_{beat} =$ 304.9234 GHz $\pm$ 150 kHz, where l =10 and $f_{EO} =$ 31.16323 GHz utilizing (3). The fluctuations observed in the repetition rate of the DKS are attributed to a series of factors, including mechanical fluctuations of the tapered fibers that are used to couple light into the microresonator, which introduces perturbations in the amount of optical power coupled into the microresonator.

The second half of the power from the electro-optic division chain is to match two of the electro-optically-divided tones from the DKS to a harmonic of the MLL-PIC's repetition rate frequency, in this case the 18th harmonic following $f_{inj} = 18 f_{rep}$. To achieve this goal, the second set of axial modes in the EOD chain are isolated using a second waveshaper. Therefore, the offset frequency becomes ($f_{offset} = 2 f_{EO} =$ 62.326460 GHz),

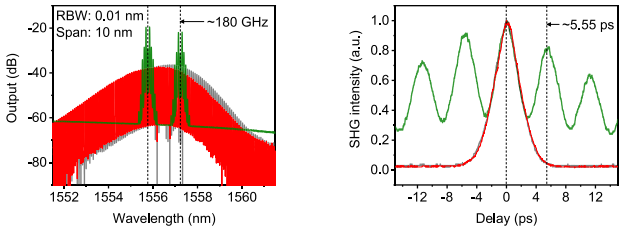

Fig. 5. Optical output of DKS after EOD and MLL-PIC before and after f_{inj} ~180 GHz RHIL. (a) Optical spectrum of DKS (olive), MLL-PIC under PML (gray) and MLL-PIC after RHIL (red). (b) SHG pulse intensity autocorrelation of DKS after EOD (green) and MLL-PIC before (gray) and after (red) RHIL.

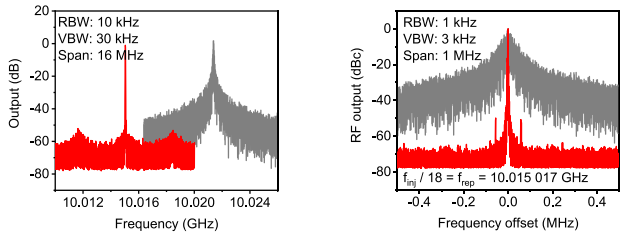

Fig. 6. RF output of MLL-PIC before and after 180 GHz RHIL. (a) RF spectrum of MLL-PIC under PML (gray) and MLL-PIC after RHIL (red) on a 10 MHz span. (b) RF spectrum of MLL-PIC under PML (gray) and MLL-PIC after RHIL (red) on a 1 MHz span where both datasets are plotted relative to their respective peak frequencies.

using (1), this results in,

$$f_{inj} = \nu_{rep} - 2f_{offset} = 304.9234\ \text{GHz} \pm 150\ \text{kHz}$$
$$-2(62.32646\ \text{GHz}) = 180.2705\ \text{GHz} \pm 150\ \text{kHz}. \quad (5)$$

The optical spectrum of the isolated tones with a frequency spacing of f_{inj} ~180 GHz is highlighted on Fig. 2(d). Following (2) and using $k = 18$, successful RHIL can be achieved when the repetition rate frequency of the MLL-PIC is within,

$$f_{rep-calc} = \frac{f_{inj}}{18} = 10.015028\ \text{GHz} \pm 8\ \text{kHz} \quad (6)$$

The output of the second waveshaper is amplified and launched into a Mach-Zehnder modulator (MZM), which is driven by a beat signal corresponding to the MLL-PIC's repetition rate (f_{rep}) at 10 GHz. This beat signal is initially photodetected in the intracavity absorber (IA) of the MLL-PIC, it is then amplified and used to drive the MZM. The modulated light is delayed through ~50 m of single-mode fiber (SMF) and later passed through an optical phase delay (OPD) before it is launched into the injection locking port of the MLL-PIC. This creates a COEO loop and serves to increase the cavity Q of the MLL-PIC and decreases the phase noise of the 10 GHz beat signal [18]. This consequently supports the harmonic injection locking process. In the time-domain, the COEO serves as a sinusoidal modulation signal that preferentially selects one out of 18 pulses from the injected tones, thereby improving the overall stability and robustness of the RHIL. It is important to note that the ~50 m of SMF serve to increase the optoelectronic cavity Q of the COEO, whereas the OPD serves to closely match the pulses from the Kerr-based soliton to the pulses of the MLL-PIC, while simultaneously matching a subharmonic of the FSR of the electro-optic-modulated Kerr-based soliton (f_{inj} ~180 GHz), and the MLL-PIC (f_{rep} ~10 GHz).

A. 180 GHz Optical Frequency Division Via Regenerative Harmonic Injection Locking

The optical spectrum of the injected tones from the electro-optically divided DKS at f_{inj} ~180 GHz is shown in Fig. 5(a). The optical spectrum of the MLL-PIC under passive mode-locking (PML) and after RHIL are also shown in Fig 5(a). As expected, RHIL results in distortion of the optical spectrum [15]. Similarly, the pulse intensity autocorrelation of the DKS after EOD with a repetition rate of f_{inj} ~180 GHz is shown in Fig. 5(b). It is important to note that an envelope beat with a frequency of ~10 GHz due to the COEO is clearly observed. The pulse intensity autocorrelation of the MLL-PIC under passive mode-locking (PML) as well as after RHIL are also shown in Fig. 5(b).

The RF spectrum of the MLL-PIC under PML, as well as after RHIL is shown in Fig. 6(a) over a 16 MHz span. It can be observed that the repetition rate of the MLL-PIC after RHIL shifts from 10.021 to 10.015 GHz. A clear reduction of the phase noise sidebands, as well as a suppression of over 50 dB in the COEO sidebands is observed, indicative of successful RHIL. Furthermore, by overlaying the RF spectrum of the MLL-PIC before and after RHIL, where both spectra are plotted relative to their respective peak frequencies, and using a span of 1 MHz (depicted in Fig. 6(b)), the suppression of the phase noise sidebands can be quantified to be >50 dB SNR. Using this data, we can take the measured $f_{rep} = 10.015017$ GHz and compare it to the calculated repetition rate using the electro-optically divided beat of the DKS (f_{beat}, see (6)). The difference between them is: $\delta f = 11$ kHz which is less than the expected drift of 8 kHz. This shows clear evidence that the DKS and the MLL-PIC are successfully linked using the RHIL technique.

In order to improve the repetition rate instability of the DKS (and consequently the repetition rate instability of the MLL-PIC), we implemented a technique to stabilize the electro-optically divided frequency beat of the DKS. This beat, which is linked to the repetition rate of both the DKS and MLL-PIC, is perturbed via mechanical and environmental fluctuations in our experimental setup: Such as tapered fiber mechanical fluctuations, COEO fiber length variations, polarization mixing, etcetera. This beat signal obtained by electro-optic division of the DKS is down-converted with a synthesized signal equal to $f_{beat} = 6.708950$ GHz. Then, the down-converted output serves as an error signal used as the input of a servo-box that controls the soliton's repetition rate via pump frequency detuning. This is done by adding the output of the servo-box to the input signal of the VCO driving the IQ modulator that controls the frequency detuning of the pump laser, as shown in the locking section of Fig. 3(b). The resulting beat signal oscillates at $f_{beat} = 6.708950$ GHz and is shown in Fig. 7(a). This results in a DKS' repetition rate of $\nu_{rep} = 304.923350$ GHz.

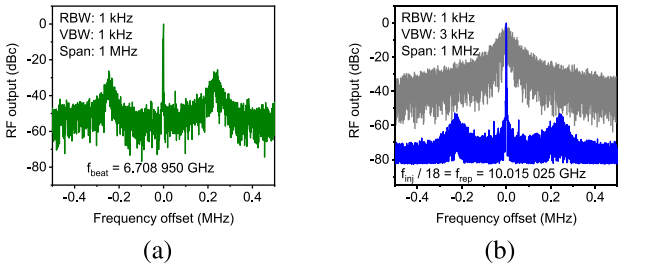

Fig. 7. RF output of MLL-PIC and DKS with a locked repetition rate. (a) RF spectrum of DKS beat (olive). (b) RF spectrum of MLL-PIC under PML (gray) and MLL-PIC after RHIL (blue) on a 1 MHz span where both datasets are plotted relative to their respective peak frequencies.

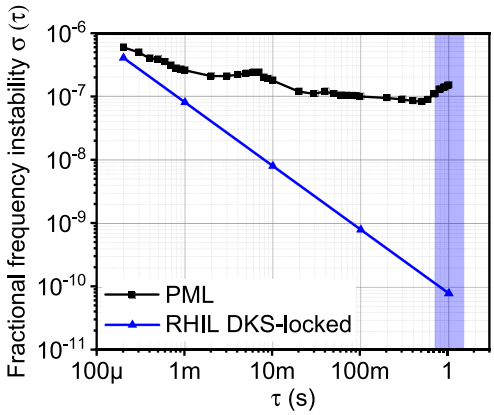

Fig. 8. Repetition rate frequency instability (Allan deviation) of the MLL-PIC under PML (black) and after RHIL link (f_{inj} ~180 GHz) with DKS (blue) where the DKS repetition rate was locked using the f_{beat} signal.

The repetition rate beat of the MLL-PIC under PML and after RHIL is shown in Fig. 7(b) centered around its carrier frequency in a 1 MHz span. The measured repetition rate is $f_{rep} = 10.015025$ GHz. The sidebands at ± 240 kHz are directly inherited from the repetition rate lock from Fig. 7(a). Using (1) and (2) the calculated MLL's repetition rate must oscillate at a frequency of $f_{rep} = 10.015024$ GHz. If we compare this calculation to the measurement shown in Fig. 7(b), the difference is 1 kHz, which is limited by the resolution bandwidth used in the measurement (RBW = 1 kHz).

Finally, we measure the repetition rate frequency instability of the MLL-PIC to confirm that it inherits the instability limit that is imposed by the synthesizer at f_{beat} that locks the repetition rate frequency of the DKS. This measurement was performed by counting the repetition rate beat signal of the MLL-PIC using a zero-dead time frequency counter. Using the frequency counter data. the Allan deviation is computed and plotted in Fig. 8. As shown, it follows a $1/\tau$ trend indicative of white phase noise and limited by the digits of precision of the frequency counter at 10^{-10} at 1 s, which corresponds to a frequency instability of 1 Hz in a 10 GHz carrier. Based on observations in [15], we anticipate that a more precise measurement could show an instability of 10^{-12} at 1 second, corresponding 10 mHz in a 10 GHz carrier.

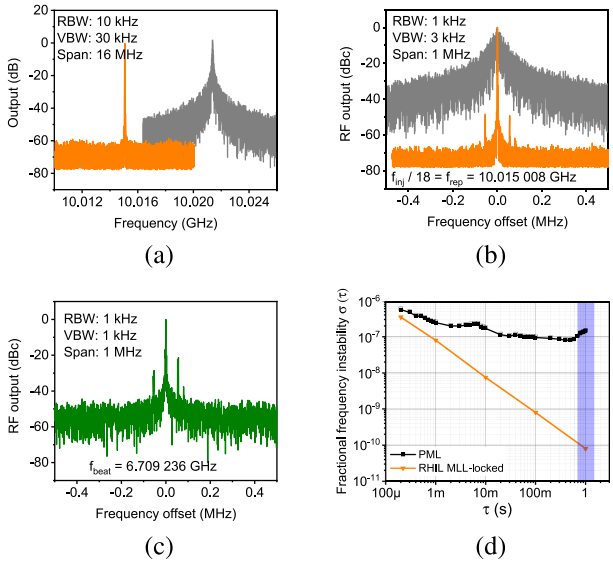

Fig. 9. RF output of DKS and MLL-PIC before and after 180 GHz RHIL. (a) RF spectrum of MLL-PIC under PML (gray) and MLL-PIC after RHIL (orange) on a 10 MHz span. (b) RF spectrum of MLL-PIC under PML (gray) and after RHIL (orange) on a 1 MHz span where both datasets are plotted relative to their respective peak frequencies. (c) EOD beat of DKS after repetition rate lock (olive). (d) MLL-PIC repetition rate instability (Allan Deviation) under PML (black) and after RHIL link (f_{inj} ~180 GHz) with DKS (orange), where the DKS repetition rate was locked using the f_{rep} signal.

B. 180 GHz Kerr Comb Repetition Rate Lock Via Regenerative Harmonic Injection Locking

Perhaps a more interesting application of RHIL is to use the beat signal of the repetition rate frequency of the MLL-PIC (f_{rep}) to simultaneously measure and stabilize the repetition rate of the DKS (ν_{rep}). The experimental setup is similar to the locking section of Fig. 3(b), but instead of down-converting the EOD beat signal from the DKS f_{beat}, we down-convert f_{rep} and use that as a feedback point to control the repetition rate of the DKS and MLL-PIC simultaneously via detuning the frequency of the pump laser used to generate the DKS. The experimental setup is shown in the locking section (c) of Fig. 3.

The RF spectrum of the MLL-PIC over a 10 MHz span under PML and after RHIL is shown in Fig. 9(a), where a clear reduction of the phase noise sidebands as well as COEO sidebands is observed. Furthermore, we plot the same data over a 1 MHz span in Fig. 9(b), where PML and RHIL are centered around their respective peak frequencies. The repetition rate of the MLL-PIC after RHIL is defined by the lock at $f_{rep} = 10.015008$ GHz. The EOD-beat of the DKS is depicted in Fig. 9(c) with a measured beat frequency at $f_{beat} = 6.709236$ GHz. It is important to note that the two beats mimic each other, which show strong evidence of mutual synchronization between the repetition rates of the MLL-PIC and the DKS.

Taking (1), (2), and (3) the repetition rate of the DKS is calculated to be $\nu_{rep} = 304.923064$ GHz. Furthermore the calculated repetition rate of the MLL-PIC must be $f_{rep} = 10.015008$ GHz, whereas the imposed one is $f_{rep} = 10.015008$ GHz. This results in a difference of $\delta f = 0$ Hz which is limited by the resolution bandwidth of the measurement (1 kHz). This effectively proves

that it is possible to link and measure the repetition rate of a DKS using a MLL-PIC via RHIL. Furthermore, is proves that this technique can provide a feedback signal that serves to simultaneously stabilize the repetition rates of both DKS and the MLL-PIC (ν_{rep} and f_{rep}).

Finally, we measured the repetition rate's fractional frequency instability and calculated the Allan deviation of the repetition rate of the MLL-PIC, the results are shown in Fig. 9(d). Similar to the results shown in previous sections, the $1/\tau$ trend as well as the limit of 10^{-10} at 1 s show definitive proof that we can simultaneously stabilize both the DKS and the MLL's repetition rates.

IV. Conclusion

In this work, we have presented an optical frequency division technique that divides a microresonator frequency comb with a repetition rate of 305 GHz down to 180 GHz using electro-optic division and then to 10 GHz (division by 18) using regenerative harmonic injection locking with an MLL-PIC. Our calculations show that the frequency division is accurate, since the difference between our measurements (using RHIL and the MLL-PIC) is smaller than the natural fluctuations of the repetition rate of the DKS. Furthermore, we stabilize the repetition rate of the DKS using EOD and measure the instability limit through the MLL, achieving a fractional frequency instability in the repetition rate of the MLL-PIC of 10^{-10} at 1 second average time, limited by the precision of the frequency counter. Finally, we utilize the repetition rate beat signal of the MLL-PIC to stabilize the repetition rate of the DKS, achieving a fractional frequency instability limit in the MLL-PIC of 10^{-10} at 1 second average time, where the difference in our measurements are smaller than the resolution bandwidth of the measurement itself. Future improvements of our experiment could include the replacement of the multiple phase modulators used for electro-optic division with a single high-voltage phase-modulator. Also, integrating the electro-optic modulators into a thin-film Lithium Niobate platform or even InP-based platform could greatly increase the long-term stability of our technique and achieve the goal of a fully integrated optical frequency comb. To the best of our knowledge, this is the first time where the frequency combs generated by a chip-scale microresonator and an integrated semiconductor mode-locked laser have been synchronized. This could enable future compact optical frequency comb applications, such as frequency metrology or optical atomic clocks.

References

[1] P. J. Delfyett *et al.*, "Optical frequency combs from semiconductor lasers and applications in ultrawideband signal processing and communications," *J. Lightw. Technol.*, vol. 24, no. 7, pp. 2701–2719, Jul. 2006.

[2] T. Udem, J. Reichert, R. Holzwarth, and T. Hänsch, "Absolute optical frequency measurement of the cesium D1 line with a mode-locked laser," *Phys. Rev. Lett.*, vol. 82, no. 18, pp. 3568–3571, 1999.

[3] S. A. Diddams *et al.*, "An optical clock based on a single trapped ^{199} Hg^{+} ion," *Science*, vol. 293, no. 5531, pp. 825–828, Aug. 2001.

[4] P. Marin-Palomo *et al.*, "Microresonator-based solitons for massively parallel coherent optical communications," *Nature*, vol. 546, no. 7657, pp. 274–279, 2017.

[5] M. U. Piracha *et al.*, "Range resolved lidar for long distance ranging with sub-millimeter resolution," *Opt. Express*, vol. 18, no. 7, pp. 7184–7189, Mar. 2010.

[6] D. T. Spencer *et al.*, "An optical-frequency synthesizer using integrated photonics," *Nature*, vol. 557, no. 7703, pp. 81–85, May 2018.

[7] P. J. Delfyett, I. Ozdur, N. Hoghooghi, M. Akbulut, J. Davila-Rodriguez, and S. Bhooplapur, "Advanced ultrafast technologies based on optical frequency combs," *IEEE J. Sel. Topics Quantum Electron.*, vol. 18, no. 1, pp. 258–274, Jan./Feb. 2012.

[8] T. J. Kippenberg, A. L. Gaeta, M. Lipson, and M. L. Gorodetsky, "Dissipative Kerr solitons in optical microresonators," *Science*, vol. 361, no. 6402, Aug. 2018, Art. no. eaan8083.

[9] S. A. Diddams, "The evolving optical frequency comb," *J. Opt. Soc. Amer. B*, vol. 27, no. 11, pp. B 51–B60, 2010.

[10] J. Reichert, R. Holzwarth, T. Udem, and T. W. Hänsch, "Measuring the frequency of light with mode-locked lasers," *Opt. Commun.*, vol. 172, no. 1, pp. 59–68, Dec. 1999.

[11] M. Malinowski *et al.*, "Towards on-chip self-referenced frequency-comb sources based on semiconductor mode-locked lasers," *Micromachines*, vol. 10, no. 6, p. 391, Jun. 2019.

[12] T. E. Drake *et al.*, "Terahertz-rate Kerr-microresonator optical clockwork," *Phys. Rev. X*, vol. 9, no. 3, Aug. 2019, Art. no. 031023.

[13] B. Wang, Z. Yang, X. Zhang, and X. Yi, "Vernier frequency division with dual-microresonator solitons," *Nature Commun.*, vol. 11, no. 1, pp. 1–7, Dec. 2020.

[14] T. Tetsumoto, F. Ayano, Y. E. Mark, J. Webber, T. Nagatsuma, and A. Rolland, "300 GHz generation based on a kerr microresonator frequency comb stabilized to a low noise microwave reference," *Opt. Lett.*, vol. 45, pp. 4377–4380, Jun. 2020.

[15] R. Bustos-Ramirez, L. R. Trask, A. Bhardwaj, G. E. Hoefler, F. A. Kish, and P. J. Delfyett, "Direct chip-scale optical frequency divider via regenerative harmonic injection locking," *Opt. Lett.*, vol. 46, no. 4, pp. 908–911, Feb. 2021.

[16] R. Adler, "A study of locking phenomena in oscillators," *Proc. IEEE*, vol. 61, no. 10, pp. 1380–1385, Oct. 1973.

[17] W. Lee and P. J. Delfyett, "Dual-mode injection locking of two independent modelocked semiconductor lasers," *Electron. Lett.*, vol. 40, no. 19, pp. 1182–1183, 2004.

[18] R. Bustos-Ramirez *et al.*, "Repetition rate stabilization and optical axial mode linewidth reduction of a chip-scale MLL using regenerative multitone injection locking," *J. Lightw. Technol.*, vol. 36, no. 14, pp. 2948–2954, Jul. 2018.

[19] A. Bhardwaj *et al.*, "A monolithically integrated racetrack colliding-pulse mode-locked laser with pulse-picking modulator," *IEEE J. Quantum Electron.*, vol. 56, no. 4, pp. 1–8, Aug. 2020, Art no. 20000708.

[20] T. C. Briles, S. P. Yu, T. E. Drake, J. R. Stone, and S. B. Papp, "Generating octave-bandwidth soliton frequency combs with compact low-power semiconductor lasers," *Phys. Rev. Appl.*, vol. 14, no. 1, Jul. 2020, Art. no. 014006.

[21] P. Del'Haye, S. B. Papp, and S. A. Diddams, "Hybrid electro-optically modulated microcombs," *Phys. Rev. Lett.*, vol. 109, no. 26, Dec. 2012, Art. no. 263901.